Adaptive Feedforward Control for DC/DC Converters in Microgrids – A Power Hardware in the Loop Study

Jan Wachter
Institute for Automation and Applied Informatics (IAI)
Karlsruhe Institute of Technology
Karlsruhe, Germany
jan.wachter@kit.edu

Lutz Gröll
Institute for Automation and Applied Informatics (IAI)
Karlsruhe Institute of Technology
Karlsruhe, Germany
lutz.groell@kit.edu

Veit Hagenmeyer
Institute for Automation and Applied Informatics (IAI)
Karlsruhe Institute of Technology
Karlsruhe, Germany
veit.hagenmeyer@kit.edu

Abstract—This paper presents the application of an adaptive feedforward control approach based on radial basis functions for grid-tied Ćuk converters. A stability analysis provides a theoretical foundation for the expected stable operating range as well as bounds for the control signal at the operating points. With a power hardware in the loop implementation of the approach the feasibility for real-time application is shown, which is further illustrated by operating scenarios. Further, practical experience concerning the choice of the control parameters is presented along with the resulting advantages and limitations of the approach.

Keywords—microgrid, power hardware in the loop testbench, adaptive control

I. Introduction

Increasing efforts towards carbon neutrality require the incorporation of renewable distributed energy resources (DER), which calls for novel control methods in combination with adjusted grid topologies. This has inherent challenges in terms of control, stability and reliability for the electric energy system [1], [2]. Testbenches are of utmost importance to ease the transition from computer simulation to field testing. For early stage assessment of the suitability of new control approaches, the use of power hardware in the loop (PHIL) systems is common [3]–[5], but has its own challenges, arising from communication delays and restrictions posed by the real-time implementation in terms of computational complexity.

Adaptive control methods offer advantages for systems with uncertainties and systems which are exposed to changing exogenous conditions. Converters in electric grids are such systems for various reasons: mass production related variations in the parameters of the electric components such as inductors or capacities, changing grid topology resulting from the intermittency of renewable energy resources as well as the changing load conditions which occur in electric grids.

However, adaptive control methods, aside from gain scheduling, are seldom used in practical applications. This is due to various destabilising phenomena such as peaking, bursting or parameter drift, which can suddenly arise during operation [6]. For linear systems, the stability of some adaptive control systems can be shown under certain strict assumptions, which can not be easily transferred to nonlinear systems. Even for linear systems, counterexamples show that the presence of unmodeled fast dynamics can lead to instabilities for adaptive controllers [7]. Since the control design for converter systems is mostly based on averaged models, which neglect the switching nature of such systems, fast unmodeled dynamics are certainly present during the operation.

With these conditions in mind, we approach this topic using a self-learning/data-driven [8] adaptive feedforward control method, which due to its single loop architecture is expected to behave robustly. Further, the straight forward implementation and low computational complexity make it well suited for real-time applications.

To gain insights in the stability properties of such systems, we choose a well studied converter topology, the Ćuk converter, for which many control approaches and validated models exist which provide valuable model knowledge, cf. [9]–[11] and the references therein. Moreover, the consideration of duty cycle controlled converters with the inherent limitation of the control signal makes this approach less susceptible to peaking phenomena and simplifies theoretical considerations by providing limits for the adapted parameters.

To assess the properties of the developed adaptive feedforward control (AFC) method in a real-time application, several scenarios for the DC bus voltage regulation in an example microgrid based on power hardware in the loop (PHIL) emulation devices are considered.

The remainder of this paper is structured as following, Sec. II presents the system under study and the assumptions made. In Sec. III the implemented control method is described and Sec. IV provides insights into the stability properties of the closed loop system. Section V discusses the obtained results and Sec. VI summarizes the paper.

II. System under Study

An example microgrid with an AC/DC interconnection is shown in Fig. 1, which is abstracted for the experiments
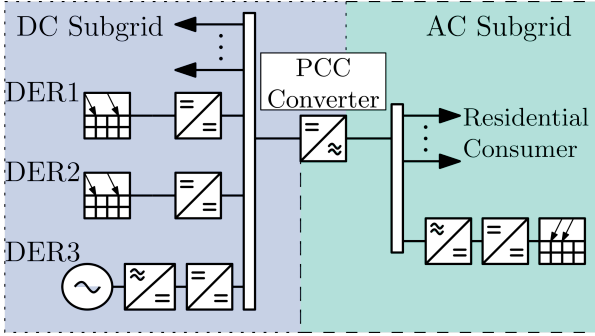
Fig. 1. Illustrative interconnected microgrid

presented in Sec. V with the following assumptions:

- **DC Subgrid:** The DC/DC converters connecting the DER are Ćuk converters with unknown parameter sets. Further we neglect the dynamics of the generation side.
- **Connection DC/AC:** The converter at the point of common coupling (PCC) is assumed to be tightly droop controlled. This allows us to model it as a combined constant resistance and constant power representation. Unidirectional power flow from the DC to the AC subgrid is assumed.
- **Devices:** Two supply converters CC1, CC2 and the PCC converter are considered for the PHIL validation setup, resulting in the system shown in Fig. 2.
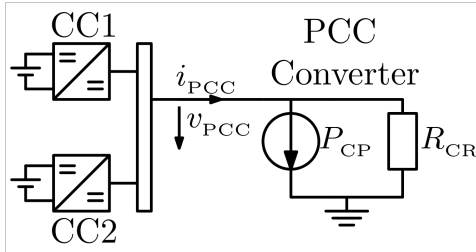
Fig. 2. System overview with respect to the assumptions made

A. Model of the Ćuk Converter

From the circuit diagram of the Ćuk converter in Fig. 3, the following equations [9] are obtained using Kirchhoff's laws

$$
\begin{aligned}
L_1 \frac{di_1}{dt} &= -(1 - s_1)v_2 + V_{\text{sup}} \\
C_2 \frac{dv_2}{dt} &= (1 - s_1)i_1 + s_1 i_3 \\
L_3 \frac{di_3}{dt} &= -s_1 v_2 - v_4 \\
C_4 \frac{dv_4}{dt} &= i_3 - i_{\text{load}},
\end{aligned}
\tag{1}
$$

where v, i represent the voltages and currents, C, L denote
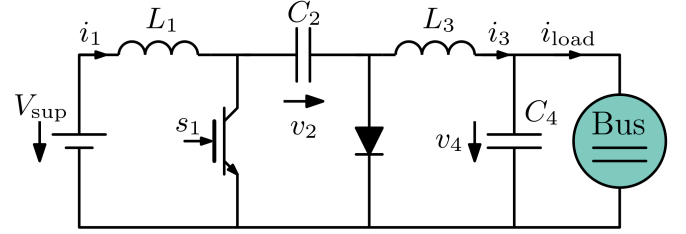
Fig. 3. Circuit diagram of a grid connected Ćuk converter

the capacitance and inductance of the corresponding passive elements, V_{sup} is the supply voltage and s_1 the gate signal of the electric switch. In the following, we interpret the signals of (1) as averaged over one period of the pulse width modulation frequency, justifying the assumption that the sliding average of s_1 can be approximated by the duty cycle d [9], [12]. Note that the model only describes the continuous conduction mode [10]. For the control design, system (1) is mapped to control nomenclature as given in Table I. Based on the mapping the following representation is obtained:

$$
\begin{aligned}
\dot{x} &= \begin{bmatrix} p_1(-x_2 + p_5) \\ p_2 x_1 \\ -p_3 x_4 \\ p_4 x_3 \end{bmatrix} + \begin{bmatrix} p_1 x_2 \\ p_2(-x_1 + x_3) \\ -p_3 x_2 \\ 0 \end{bmatrix} u + \begin{bmatrix} 0 \\ 0 \\ 0 \\ -p_4 \end{bmatrix} z \\
y &= \begin{bmatrix} 0 & 0 & 0 & -1 \end{bmatrix} x.
\end{aligned}
\tag{2}
$$

TABLE I
MAPPING TO CONTROL NOTATION

Name	Physical Notation	Control Notation
States	i_1, v_2, i_3, v_4	x_1, x_2, x_3, x_4
Input	d	u
Output	$-v_4$	y
Disturbance	i_{load} (measured)	z
Parameters	L_1, C_2	$p_1 = \frac{1}{L_1}$, $p_2 = \frac{1}{C_2}$
	L_3, C_4	$p_3 = \frac{1}{L_3}$, $p_4 = \frac{1}{C_4}$
	V_{sup}	$p_5 = V_{\text{sup}}$

B. Model of the Point of Common Coupling Converter

Following the assumptions given in Sec. I, we model the PCC current i_{PCC} as consisting of a constant resistance and a constant power component as shown in Fig. 2. This yields

$$
i_{\text{PCC}} = \frac{P_{\text{CP}}}{v_{\text{PCC}}} + \frac{v_{\text{PCC}}}{R_{\text{CR}}},
\tag{3}
$$

where v_{PCC} is the PCC voltage, R_{CR} the constant resistance and P_{CP} the constant power. Due to the unidirectional power flow, the PCC current is considered as a load during the validation scenarios.

III. Adaptive Feedforward Control Design for the Ćuk Converters

Adaptive feedforward control approaches, for example Adaptive Inverse Control (AIC) [13], are well established

in engineering practice, since they offer robust performance and easy implementation for stable plants [14], [15]. The underlying idea is to adapt the feedforward controller to approximate an inverse of the plant [16]. Various methods based on different identification/filtering approaches and/or model reference based concepts are described in [14]–[17]. To provide the desired bus voltage, we use a feedforward controller, as shown in Fig. 4, based on a radial basis function (RBF) network. However, we do not aim to approximate the plant inverse as in [14], [16]. Since we are only interested in a setpoint control application we want to obtain the static characteristic of the plant. Consequently, the RBF network acts as a static nonlinear feedforward controller, whose parameters are adjusted via the adaptation loop to guarantee zero steady state error. Decentralized load sharing is achieved by modifying the AIC structure with a virtual resistance based disturbance feedforward to the controller input. The activation of the kernels is based on the desired output and thus can be interpreted in the sense of gain scheduling. According to AIC and the scheme in Fig. 4, the kernel weights are adapted based on the tracking error e which is given by

$$e = y - y_d \,. \tag{4}$$
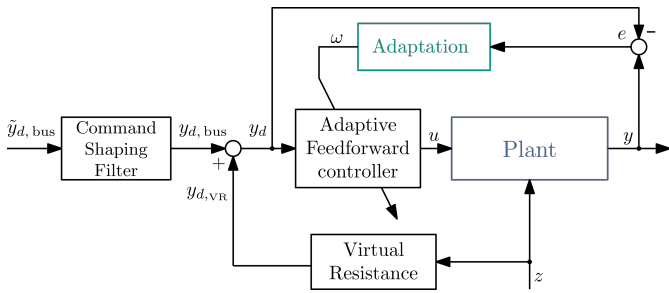
Fig. 4. Overview of the adaptive feedforward control scheme

The feedforward controller of the AFC is given by

$$u(y_d) = \sum_{i=1}^{l} \omega_i \, k(y_d, y_{\mathrm{vc},i}) \,, \tag{5}$$

where ω_i are the weights, k the kernel function, y_d the desired output and $y_{\mathrm{vc},i}$ the predefined kernel centers. The RBF [18], [19] is given as

$$k(y_d, y_{\mathrm{vc},i}) = \exp\left(-\frac{(y_d - y_{\mathrm{vc},i})^2}{2\,\rho^2}\right) \,, \tag{6}$$

where ρ is the kernel bandwidth. Since u is the duty cycle, it can only take values in the interval $[0, 1)$. For practical reasons the interval is reduced to $u \in [0, u_{\max})$, with $u_{\max} < 1$. Such a constraint can be realized using an adjusted saturation function, but additionally in adaptive control it should be preferred also to constrain the parameters ω. This can be achieved by a projection onto the allowed parameter range. To derive a suitable weight update we consider the gradient

descent for the quadratic tracking error J

$$J = \frac{1}{2}\big(\underbrace{y - y_d}_{=e}\big)^2 \tag{7}$$

which is given by

$$\dot{\omega}_i = -\gamma_\omega \frac{\partial J}{\partial \omega_i} \,, \tag{8}$$

with the adaptation gain $\gamma_\omega > 0$. After the initial transient, which we neglect due to small γ_ω and therefore slow parameter dynamics, the system output will settle to its stationary value $y \approx \varphi(u)$. Applying the chain rule yields

$$\begin{aligned}
\dot{\omega}_i &= -\gamma_\omega \frac{\partial J}{\partial y} \frac{\partial y}{\partial u} \frac{\partial u}{\partial \omega_i} \\
&= -\gamma_\omega e \frac{\partial \varphi(u)}{\partial u} k(y_d, y_{\mathrm{vc},i}) \,,
\end{aligned} \tag{9}$$

where $\frac{\partial \varphi(u)}{\partial u}$ is the slope of the static characteristic. With the assumption that the expected characteristic is monotone, we replace this slope with a positive constant, which we subsequently include in γ_ω. This leads to the following adaptation law supplemented with the parameter projection

$$\dot{\omega}_i = \mathrm{Proj}_{[0, \omega_{i,\max}]}\Big(-\gamma_\omega \, e \, k(y_d, y_{\mathrm{vc},i})\Big) \,. \tag{10}$$

Decentralized load sharing between the converters is realized with the disturbance feedforward law

$$y_{d,\mathrm{VR}} = -\alpha_{\mathrm{VR}} \, z \,, \tag{11}$$

where α_{VR} acts as a virtual resistance [20]–[22]. The choice of α_{VR} for CC1 and CC2 can be used to shape the load sharing ratio. Note that unmodeled additional resistances can deteriorate the designed load sharing. One example are the connection lines between the converter and the PCC, depending on the length; their respective effects can be tolerated or compensated if additional knowledge is available.

A command shaping filter is designed as a PT1 element with the time constant T_{CSF} to smooth jumps of the desired bus voltage.

The desired signal y_d for the adaptive feedforward controller is given by

$$y_d = y_{d,\mathrm{bus}} + y_{d,\mathrm{VR}} \,, \tag{12}$$

where $y_{d,\mathrm{bus}}$ is the default bus voltage. In a classical hierarchical control system, $y_{d,\mathrm{bus}}$ is provided by some higher level controller, often called secondary control [21], [23], [24]. Consequently the presented approach is to be understood as a primary control scheme. For the scenarios described in this paper, the desired bus voltage is given by the design of the experiment.

IV. STABILITY ANALYSIS

To provide a meaningful analysis of the stability of the presented approach we make the following assumptions

- We replace the measured disturbance z by a load with the constant equivalent conductance $\theta > 0$.
- The controller input y_d is considered as constant.

We further argue concerning the dynamics of the control signal u, which is given by

$$\dot{u} = \sum_{i=1}^{l} \dot{\omega}_i \, k(y_d, y_{\mathrm{vc},i})$$

$$\stackrel{(10)}{=} \sum_{i=1}^{l} \mathrm{Proj}_{[0,\omega_{i,\max}]} \left(-\gamma_\omega \, e \, k(y_d, y_{\mathrm{vc},i}) \right) k(y_d, y_{\mathrm{vc},i}), \tag{13}$$

that it is well known from adaptive control theory that stability can be proven without the projection operator, therefore we neglect it. Moreover we replace the error with the state coordinate and introduce the new gain γ which yields

$$\dot{u} \stackrel{(4)}{=} (x_4 + y_d) \underbrace{\sum_{i=1}^{l} \gamma_\omega \, k(y_d, y_{\mathrm{vc},i})^2}_{=\gamma} \tag{14}$$

and thus justifies the aggregation of the weights in the control signal u.

Interpreting u as a new state variable, the extended dynamics for $x = [x_1 \ \ x_2 \ \ x_3 \ \ x_4 \ \ u]^\top$ is given by

$$\dot{x} = \begin{bmatrix} p_1(-x_2 + x_2 u + p_5) \\ p_2(x_1 - x_1 u + x_3 u) \\ p_3(-x_4 - x_2 u) \\ p_4(x_3 - \theta x_4) \\ \gamma(x_4 + y_d) \end{bmatrix}. \tag{15}$$

We can obtain the following equilibrium set

$$\mathcal{E}_x = \left\{ \begin{bmatrix} \frac{\theta y_d^2}{p_5} \\ p_5 + y_d \\ -\theta y_d \\ -y_d \\ \frac{y_d}{y_d + p_5} \end{bmatrix} : y_d \in \mathbb{R}^+ \right\}, \tag{16}$$

note that $u_e = \frac{y_d}{y_d + p_5}$. We apply the equilibrium transformation $\tilde{x} := x - x_e$, $\tilde{u} := u - u_e$ which yields

$$\dot{\tilde{x}} = A(\tilde{u}) \, \tilde{x} \tag{17}$$

$$A = \begin{bmatrix} 0 & p_1(\tilde{u} - \beta_1) & 0 & 0 & p_1 \beta_3 \\ p_2(\beta_1 - \tilde{u}) & 0 & p_2(\tilde{u} + \beta_2) & 0 & -p_2 \beta_4 \\ 0 & -p_3(\tilde{u} + \beta_2) & 0 & -p_3 & -p_3 \beta_3 \\ 0 & 0 & p_4 & -p_4 \theta & 0 \\ 0 & 0 & 0 & \gamma & 0 \end{bmatrix},$$

with $\beta_1 = \frac{p_5}{p_5 + y_d}$, $\beta_2 = \frac{y_d}{p_5 + y_d}$, $\beta_3 = (p_5 + y_d)$, $\beta_4 = \frac{\theta \, y_d (p_5 + y_d)}{p_5}$.

We treat the above pseudo-linear problem caused by the variable $\tilde{u}$ by embedding it in an LTV system of the structure

$$\dot{\tilde{x}} = A(t)\tilde{x}, \tag{18}$$

where the time-varying matrix $A(t)$ can be expressed by $A(t) = A_0 + \tilde{u}(t) \, B$, with the matrices A_0 and B, which

are given by

$$A_0 = \begin{bmatrix} 0 & -p_1 \beta_1 & 0 & 0 & p_1 \beta_3 \\ p_2 \beta_1 & 0 & p_2 \beta_2 & 0 & -p_2 \beta_4 \\ 0 & -p_3 \beta_2 & 0 & -p_3 & -p_3 \beta_3 \\ 0 & 0 & p_4 & -p_4 \theta & 0 \\ 0 & 0 & 0 & \gamma & 0 \end{bmatrix}$$

$$B = \begin{bmatrix} 0 & p_1 & 0 & 0 & 0 \\ -p_2 & 0 & p_2 & 0 & 0 \\ 0 & -p_3 & 0 & 0 & 0 \\ 0 & 0 & 0 & 0 & 0 \\ 0 & 0 & 0 & 0 & 0 \end{bmatrix}. \tag{19}$$

The time-varying matrix $A(t)$ is unknown, but lies in a convex set, i.e. $A(t) \in \{A_0 + \tilde{u}(t)B : \tilde{u} \in [\underline{u}, \overline{u}]\}$ with $\underline{u}, \overline{u}$ as the lower and upper admissible bounds. Let us consider the case $\overline{u} = -\underline{u} = \alpha$ to obtain symmetric bounds for $\tilde{u}$ about its equilibrium value. Now we search the largest α for which we can guarantee stability. Taking a time independent Lyapunov function candidate $V(\tilde{x}) = \tilde{x}^\top P \tilde{x}$ with $P \succ 0$ it has to be shown that

$$A^\top(t)P + PA(t) \prec 0, \quad \underbrace{A_0 - \alpha B}_{\underline{A}} < A(t) < \underbrace{A_0 + \alpha B}_{\overline{A}}. \tag{20}$$

This task can be reduced to the problem of finding a common Lyapunov function for the corner matrices $\underline{A}, \overline{A}$. Hence, we obtain the following optimization problem

$$\max_{\alpha,P} \alpha \ \text{s.t.} \ (A_0 + \alpha B)^\top P + P(A_0 + \alpha B) \prec 0$$

$$(A_0 - \alpha B)^\top P + P(A_0 - \alpha B) \prec 0 \tag{21}$$

$$-P \prec 0.$$

Due to the strict inequalities as well as bilinear relation between α and P a sequence of feasibility problems with fixed α has to be solved

$$t_{\mathrm{opt}} = \min_{t,P} t \ \text{s.t.} \ (A_0 + \alpha B)^\top P + P(A_0 + \alpha B) \preceq t I_n$$

$$(A_0 - \alpha B)^\top P + P(A_0 - \alpha B) \preceq t I_n \tag{22}$$

$$-P \preceq t I_n.$$

For any $t_{\mathrm{opt}} < 0$ this problem is feasible, consequently we can optimize (21) by simply increasing α until the feasibility fails.

The result of the optimization for the parameters of CC1 and $\theta = \frac{1}{6}$ is shown in Fig. 5 by the bounds $u_{\mathrm{b}1}$. Obviously, the calculated stability region is the interior enclosed by the boundary lines, because $\alpha_{\max}$ of (21) for each u_e is only a supremum (the maximum can not be achieved, due to the strict inequalities).

Even if the stability region seems small, in practice the bounds prove to be conservative. Nevertheless, the decrease for low and high values of u_e is observed during the application of the control scheme.

Larger stability regions can be obtained by considering a slowly varying $\tilde{u}(t)$, which is achievable with $\gamma \ll 1$. Assuming that $|\dot{\tilde{u}}(t)| \leq \rho_{\tilde{u}}$, we use the linear matrix inequality

Stability Bounds on Control Signal
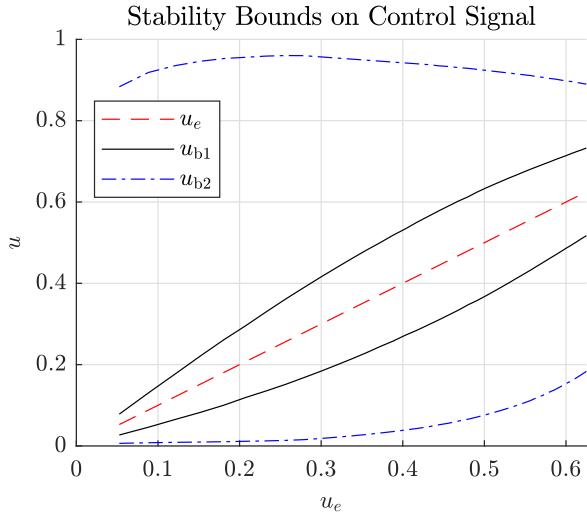
Fig. 5. Bounds on u that guarantee the existence of a common Lyapunov function

(LMI) formulation presented by Montagner and Peres [25]. For this we rewrite system (18) as

$$\dot{\tilde{x}} = (\alpha(t)A_1 + (1 - \alpha(t))A_2)\,\tilde{x}, \quad \alpha(t) \in [0,1], \qquad (23)$$

where $A_1 = A_0 + \underline{u}B$ and $A_2 = A_0 + \overline{u}B$ with symmetric relative deviations $\underline{u} = -\delta u_{\mathrm{e}}$ and $\overline{u} = \delta(1 - u_{\mathrm{e}})$. The time-varying parameter $\alpha(t) = \frac{\tilde{u}(t) - \underline{u}}{\overline{u} - \underline{u}}$ is limited to a rate of change $|\dot{\alpha}(t)| \leq \frac{\rho_{\tilde{u}}}{\delta} =: \rho_\alpha$. A time-dependent Lyapunov function

$$V(\tilde{x}, t) = \tilde{x}^\top \left(\alpha(t)P_1 + (1 - \alpha(t))P_2\right)\tilde{x} \qquad (24)$$

is used, where P_1, P_2 are symmetric positive definite solutions of the LMIs

$$A_1^\top P_1 + P_1 A_1 \pm \rho_\alpha(P_1 - P_2) \prec 0$$
$$A_2^\top P_2 + P_2 A_2 \pm \rho_\alpha(P_1 - P_2) \prec 0 \qquad (25)$$
$$A_1^\top P_2 + P_2 A_1 + A_2^\top P_1 + P_1 A_2 \pm 2\rho_\alpha(P_1 - P_2) \prec 0 \,.$$

The result of the maximization of δ, such that (25) remains feasible is shown in Fig. 5 for the parameters of CC1, $\theta = \frac{1}{6}$ and $\rho_{\tilde{u}} = 1$ by the bounds $u_{\mathrm{b}2}$. It can be seen that the resulting bounds are vastly increased by the limitation of the rate of change for the control signal u. The price for a larger stability region is a decrease of the performance.

V. POWER HARDWARE IN THE LOOP SETUP AND RESULTS

The setup of the power hardware in the loop environment which is used to obtain the results presented in this section is schematically shown in Fig. 6. The AFC approach and the models of the Ćuk converters and the PCC converter, as presented in Sec. II, are implemented on a real-time simulator to obtain the responses of the emulated Ćuk converters. The signals are then emulated as real voltages/currents using high bandwidth sources, which feed the measurements back to the real-time simulator as depicted in Fig. 6. For all connection lines between the high bandwidth sources copper wires with a cross-section of $35\,\mathrm{mm}^2$ are used.

An overview of the parameters used for the experiments is provided in Table II, note that for parameters which are changed during a scenario a range is given and the values are described in more detail in the following.

In the remainder of this section, three operating scenarios are presented for which the performance of the AFC is discussed. Afterwards the key results concerning the training, positioning and bandwidth of the kernels are presented.

TABLE II
PARAMETER OVERVIEW

Category	Parameter	Value
Ćuk converter 1 (CC1)	L_1	$10\,\mathrm{mH}$
	C_2	$22\,\mu\mathrm{F}$
	L_3	$10\,\mathrm{mH}$
	C_4	$44\,\mu\mathrm{F}$
	V_{sup}	$180\,\mathrm{V}$
Ćuk converter 2 (CC2)	L_1	$10.5\,\mathrm{mH}$
	C_2	$20.9\,\mu\mathrm{F}$
	L_3	$9.5\,\mathrm{mH}$
	C_4	$46.2\,\mu\mathrm{F}$
	V_{sup}	$200\,\mathrm{V}$
PCC converter	P_{CP}	$0 - 3000\,\mathrm{kW}$
	R_{CR}	$6 - 15\,\Omega$
AFC	γ_ω	0.01
	y_{vc}	$\begin{bmatrix} 10 & 20 & 30 & \dots & 300 \end{bmatrix}$
	ρ	10
	T_{CSF}	$1\,\mathrm{s}$
	$\alpha_{VR,CC1}$	0.3
	$\alpha_{VR,CC2}$	0.5
General	Cycle time	$20 \cdot 10^{-6}\,\mathrm{s}$
	$\tilde{y}_{d,\mathrm{bus}}$	$190\,\mathrm{V}$
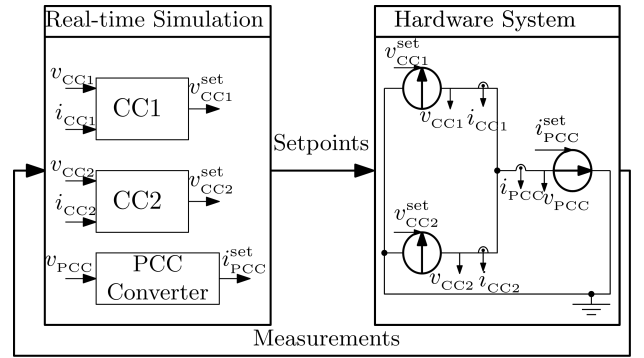
Fig. 6. Setup of the real-time PHIL environment

A. Failure of a Generation Unit

For this scenario the load parameters $R_{\mathrm{CR}} = 6.66\,\Omega$ and $P_{\mathrm{CP}} = 1000\,\mathrm{W}$ are chosen. Fig. 7 shows the transient behavior during the sudden failure of a supply converter, evident by i_{CC2} dropping to zero. The induced bus voltage drop is recovered within $0.05\,\mathrm{s}$ followed by a transient period until the new operating point is reached. Note that since the remaining converter is now contributing a larger current, consequently

the new bus voltage is lower due to the implemented virtual resistance. The magnitude of the voltage difference is quite large, due to the extreme scenario of losing over 50% of the initial supply current, indicating the robustness of the chosen approach.

Voltage at the PCC
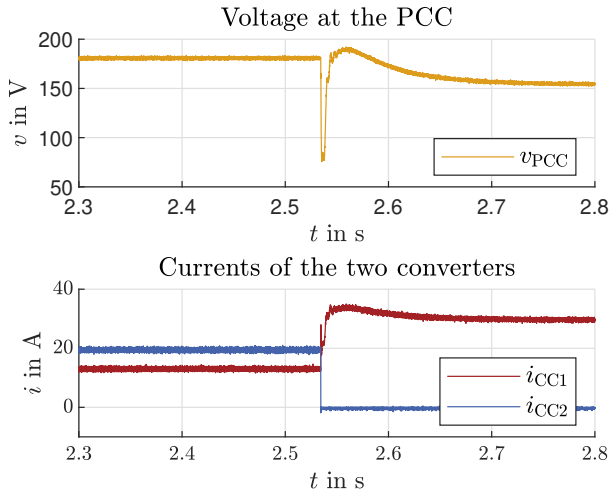
Fig. 7. Response of the bus voltage and supply currents during the failure of one converter

B. Resistive Load Change

Fig. 8 shows the behavior of the system during a step change of the load resistance R_{CR} from $13.32\,\Omega$ to $6.66\,\Omega$. Note that for this scenario, the constant power term was chosen as $P_{\mathrm{CP}} = 0$. After a transient period of around $0.02\,\mathrm{s}$ the new operating point is reached, the load sharing ratio of around $\frac{i_{\mathrm{CC1}}}{i_{\mathrm{CC2}}} = 0.61$ is maintained after the load step. Again the bus voltage after the load increase is smaller, due to the virtual resistance.
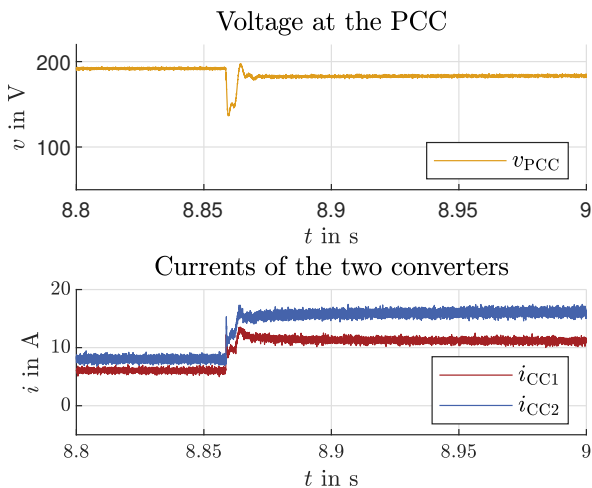
Fig. 8. Response of the bus voltage and supply currents during step change of the resistive load

C. Constant Power Load Change

In a second load change scenario, the behavior during the change of the constant power term from $P_{\mathrm{CP}} = 1000\,\mathrm{W}$ to $P_{\mathrm{CP}} = 3000\,\mathrm{W}$ is presented in Fig. 9. The resistive load component is kept constant at $R_{\mathrm{CR}} = 6.66\,\Omega$. Similar to the previous scenario, the new operating point is reached after roughly $0.03\,\mathrm{s}$ and the load sharing ratio is restored after the load change. The transient period exhibits a damped oscillatory behavior as can be expected due to the decreased damping caused by the increased constant power load share.
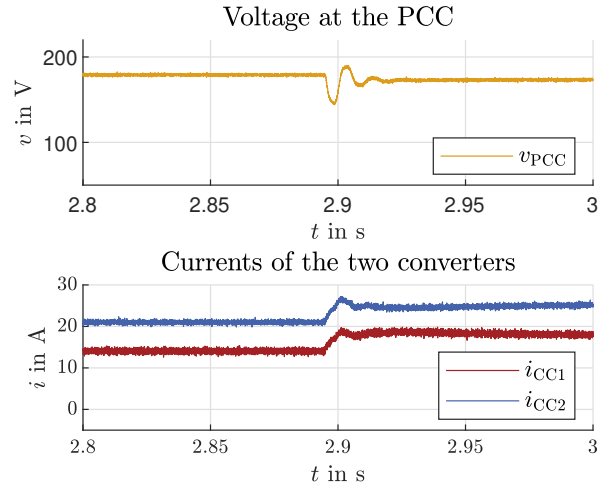
Fig. 9. Response of the bus voltage and supply currents during the change of the constant power load

D. Learning Behavior of the Kernel Weights

One of the challenges for the real-time implementation of the presented AFC method is the choice of the number and spacing of the RBF kernel centers y_{vc} in combination with the kernel bandwidth δ. The maximum number of the used kernel functions is limited by the available computational power and the minimum necessary number is limited by the desired quality of the adapted static characteristic.

For all shown scenarios the kernel centers are positioned between $10\,\mathrm{V}$ and $300\,\mathrm{V}$. A good trade-off is found to be a spacing of $10\,\mathrm{V}$ for the kernel centers in combination with a kernel bandwidth of $\delta = 10$.

In order to provide a useful static characteristic during operation, a reasonable set of weights must be obtained. The first influence to be discussed is the initialization of the weights. For all presented scenarios, the worst case is assumed and the weights are initialized as zero to evaluate the robustness of the approach with respect to ill chosen initial weights. Obviously, if a nominal static characteristic is known for the used converter type, the initial weights can be chosen accordingly to obtain better performance.

The second influence is the training of the system in order to adapt the weights to the actual conditions. The same procedure is performed for all presented scenarios. First $\tilde{y}_{d,\mathrm{bus}} = 100\,\mathrm{V}$ is

set, then CC1 is enabled, after the steady state is reached, CC2 is enabled. Thereafter $\tilde{y}_{d,\mathrm{bus}}$ is changed in $10\,\mathrm{V}$ increments up to $200\,\mathrm{V}$ with constant load conditions. Afterwards the described experiments are performed.

The approach presented above is now discussed using the three static characteristics depicted in Fig. 10:

- **Theoretical static characteristic:** a theoretical characteristic u_{ideal} for a single Ćuk converter can be obtained, assuming the knowledge of the parameters given in Table II for CC2. This curve is discussed as the reference.

- **Best approximation characteristic:** to show that the chosen number and position of kernels is sufficient to provide a good fit to the theoretical static characteristic, we calculate the best approximation for the weights with respect to the L_2-norm. The resulting characteristic u_{best} is optimized to fit the voltage range $50 - 250\,\mathrm{V}$. From a mathematical point of view, fewer kernels would be sufficient to approximate the theoretical static characteristic and also lessen the computational burden for the real-time implementation. But fewer kernels will further degrade the adapted static characteristic during operation.

- **Adapted static characteristic:** the third curve u_{CC2} is an characteristic curve obtained during operation for CC2. Evidently, the adapted static characteristic differs from the theoretically obtained curve. The monotonic behavior, inside the trained range $\approx 100 - 190\,\mathrm{V}$, as well as the value at the current operating point (depicted as the intersection of the blue and the red curve) match the theoretical prediction.
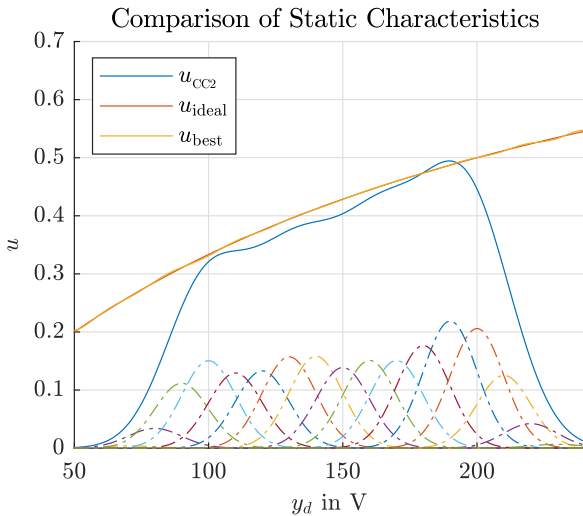
Fig. 10. Comparison of theoretical, best approximation and adapted static characteristic

To further discuss the importance of sufficient training for the weight adaption as well as the initialization of the weights, we consider the non-monotonic region depicted in Fig. 11 which shows the edge of the trained region. It becomes clear, that the system will not behave as expected for values in the untrained range, which can lead to unpredictable behavior if the system is not in a controlled training environment. This illustrates the hazards that can arise from incomplete training of such adaptive schemes. To avoid, or at least reduce such unwanted behavior, the optimization approach for the initialization of the weights as described earlier can be of great advantage if knowledge about the static characteristic is available. Further it should be noted, that due to these restrictions this scheme should only be applied if the operating range is know a priori and sufficient training can be ensured.
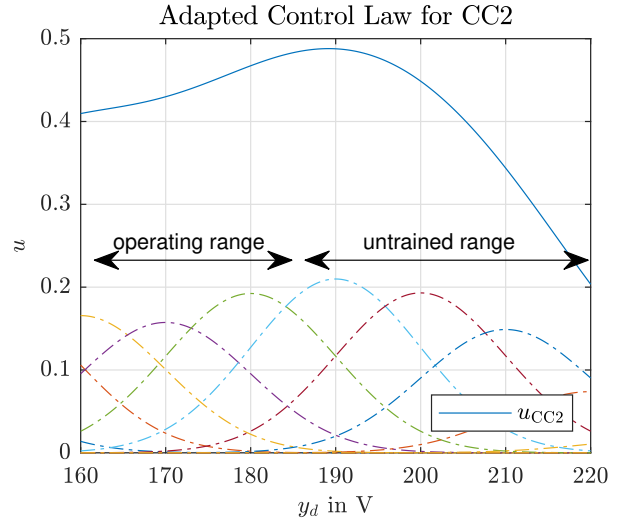
Fig. 11. Adapted static characteristic for CC2

VI. CONCLUSION AND OUTLOOK

We provide first experimental insights towards the performance of a real-time implementation of the presented adaptive feedforward control (AFC) approach during the scenarios loss of a generation unit, change of the resistive load and change of the constant power load. Further we illustrate the necessary number, positioning and training procedure of the kernel based AFC along with the arising challenges and limitations for the application of such control schemes. Additional studies need to be conducted to gain a better understanding of the modifications to implement the approach reliably with real converters in a closer-to-reality microgrid experiment.

The studied kernel based AFC scheme offers several advantages, such that only little a priori knowledge about the system is needed to implement the approach. Further, some robustness is provided by the feedforward structure and the single loop architecture. This enables a fast implementation with satisfactory behavior for a certain operating range.

The drawbacks of this approach are the inherently limited performance, which is due to the lack of model knowledge. Furthermore the stability region is limited compared to other adaptive schemes due to the absence of an inner feedback loop. The degraded performance can be partly restored by integrating model knowledge a posteriori, such as the monotonicity of the static characteristic. This additional effort lessens the advantage of the fast implementation. The stability

considerations are not simpler than for strictly model-based approaches. Lastly, the proofs tend to be more conservative when only limited system knowledge is available.

We can conclude that self-learning or data-driven adaptive control approaches can provide a quick solution for certain problems, but lose some of their promising features when they are applied to practical problems.

REFERENCES

[1] X. Wang and F. Blaabjerg, "Harmonic stability in power electronic-based power systems: Concept, modeling, and analysis", *IEEE Transactions on Smart Grid*, vol. 10, pp. 2858–2870, 2019

[2] B. Ferreira, "Understanding the challenges of converter networks and systems: Better opportunities in the future", *IEEE Power Electronics Magazine*, vol. 3, pp. 46–49, 2016

[3] V. Hagenmeyer, et al., "Information and communication technology in Energy Lab 2.0: smart energies system simulation and control center with an open-street-map-based power flow simulation example", *Energy Technology*, Wiley, vol. 4, pp. 145–162, 2016

[4] P. Kotsampopoulos, F. Lehfuss, G. Lauss, N. Bletterie and N. Hatziargyriou, "The limitations of digital simulation and the advantages of PHIL testing in studying distributed generation provision of ancillary services", *IEEE Transactions on Industrial Electronics*, vol. 62, pp. 5502–5515, 2015

[5] P. Kotsampopoulos, et al., "A benchmark system for hardware-in-the-loop testing of distributed energy resources ", *IEEE Power and Energy Technology Systems Journal*, vol. 5, pp. 94–103, 2018

[6] B. Anderson, "Failures of adaptive control theory and their resolution", *Communications in Information and Systems*, International Press of Boston, vol. 5, pp. 1–20, 2005

[7] C. Rohrs, L. Valavani, M. Athans and G. Stein, "Robustness of continuous-time adaptive control algorithms in the presence of unmodeled dynamics ", *IEEE Transactions on Automatic Control*, vol. 30, pp. 881–889, 1985

[8] Z. Hou and Z. Wang, "From model-based control to data-driven control: Survey, classification and perspective, *Information Sciences*, Elsevir, vol. 235, pp. 3-35, 2013

[9] R.W. Erickson and D. Maksimovic, *Fundamentals of power electronics*, Springer, 2007

[10] S. Ćuk, "Discontinuous inductor current in the optimum topology switching converter", *Proc. IEEE Power Electronics Specialists Conference*, pp. 105–123, 1978

[11] A. Astolfi, D. Karagiannis and R. Ortega, *Nonlinear and adaptive control with applications*, Springer, 2008

[12] A. Kastner, L. Gröll, V. Hagenmeyer, "Abstractions in modeling of switching DC/AC power converters" (in press), *Proc. LII International Scientific Conference on Control Processes and Stability (CPS)*, 2021

[13] B. Widrow and G. Plett, "Nonlinear adaptive inverse control", *Proc. 36th IEEE Conference on Decision and Control*, pp. 1032–1037, 1997

[14] J. Yao, X. Wang, S. Hu and W. Fu, "Adaline neural network-based adaptive inverse control for an electro-hydraulic servo system", *Journal of Vibration and Control*, vol. 17, pp. 2007–2014, 2011

[15] B. Widrow, *Adaptive inverse control*, Wiley-IEEE Press, 2007

[16] G. Plett, "Adaptive inverse control of linear and nonlinear systems using dynamic neural networks", *IEEE Transactions on Neural Networks*, vol. 14, pp. 360–376, 2003

[17] M. Shafiq, M.A. Shafiq and H. Yousef, "Stability and convergence analysis of direct adaptive inverse control", *Complexity*, Hindawi, vol. 2017, Article ID 7834358, 2017

[18] Y. Xiaofang, W. Yaonan, S. Wei and W. Lianghong, "RBF networks-based adaptive inverse model control system for electronic throttle ", *IEEE Transactions on Control Systems Technology*, vol. 18, pp. 750–756, 2010

[19] A. Abelli, A. Ferrari, S. Manaco and C. Richard, "Adaptive inverse control using kernel identification", *Proc. American Control Conference (ACC)*, pp. 202–207, 2012

[20] U. Tayab, M. Roslan, L. Hwai and M. Kashif, "A review of droop control techniques for microgrid", *Renewable and Sustainable Energy Reviews*, Elsevir, vol. 76, pp. 717–727, 2017

[21] Y. Wang, D. Liu, Z. Chen and P. Liu, "A hierarchical control strategy of microgrids toward reliability enhancement", *Proc. IEEE International Conference on Smart Grid*, pp. 123–128, 2018

[22] K. R. Bharath, M. K. Mithun and P. Kanakasabapathy, "A review on DC microgrid control techniques, applications and trends", *International Journal of Renewable Energy Research*, vol. 9, pp. 1328 – 1338, 2019

[23] D. Olivares, et al., "Trends in microgrid control", *IEEE Transactions on Smart Grid*, vol. 5, pp. 1905-1919, 2014

[24] N. Campagna, M. Caruso, V. Castiglia, R. Miceli and F. Viola, "Energy management concepts for the evolution of smart grids", *Proc. IEEE International Conference on Smart Grid*, pp. 208–213, 2020

[25] V. Montagner and P. Peres, "A new LMI condition for the robust stability of linear time-varying systems ", *Proc. IEEE International Conference on Decision and Control*, pp. 6133–6138, 2003